

Difference Correlators

Does Indoor Carrier Phase Tracking Allow Indoor RTK?



An indoor positioning test configuration. At left, a geodetic antenna is mounted above the pre-surveyed point, and an IFEN employee is using a software receiver to log GNSS signals.

Difference correlators represent effective means to remove signal dynamics from correlator values and to dramatically increase the coherent integration time, thus, also increasing the carrier phase tracking sensitivity. In this article, a difference correlator software algorithm is tested both indoors and in a forested area with promising new results. Findings from both single- and double-difference correlator tests are presented.

THOMAS PANY
IFEN GMBH

HANS-JUERGEN EULER
INPOSITION GMBH

JON WINKEL
IFEN GMBH

The carrier phase observable is generally considered to be the most precise GNSS measurement, yielding millimeter-level positioning accuracy outdoors. However, measuring this observable indoors or in a forest has long been thought to be impossible or, at best, very difficult.

A new carrier-tracking algorithm used in the research on which this column is based changes this situation and enables us to measure the received carrier phase even in highly degraded environments. The algorithm adapts a well-known positioning concept (single/

double difference) to the level of GNSS signal processing.

Single- and double-difference (code and carrier) correlators eliminate common mode errors and thereby reduce the signal dynamics. Applying much smaller tracking loop bandwidths or longer integration times can then reduce noise and eliminate multipath contributions during signal tracking.

For static applications, a coherent integration time of 30 seconds allows single-channel carrier tracking without cycle-slips well below zero decibel/hertz (!), provided that code and Doppler lock can be achieved by, for example, vector tracking.

This column will show that the estimated carrier phase apparently relates to the received electromagnetic wave. In forest and indoor test trials that we conducted, the carrier-phase tracking stability is extremely high and the num-

ber of cycle slips is very much smaller compared to standard phase-locked loop (PLL) tracking. Furthermore, the numerical value of the slips is small, perhaps only one cycle.

On the other hand, a received phase tracked indoors is influenced by all the possible complex propagation effects that may occur there. This complicates use of the received phase in positioning, and classical real time kinematic (RTK) positioning algorithms cannot be applied in a straightforward manner. However, a processing software that we used in our trials yields indoor positioning with about one-meter accuracy using only carrier phase data.

Difference Processing Methodology

We performed difference correlator processing using two GNSS software receivers, one acting as a rover and the other

as reference station. The data evaluation currently occurs in postprocessing but could in principle also be done in real-time.

The reference station retrieves navigation data bits of the tracked satellite signals and stores them into a file. Furthermore, the reference station generates a RINEX observation file. The rover collects intermediate frequency (IF) samples and stores them onto a hard disc.

All data from the reference station and the rover are input to the post-processing, which produces a new (improved) RINEX observation file for the rover. A data processing software then analyzes the reference and rover RINEX files to estimate the rover position.

Loosely speaking, the prompt correlator of a GNSS tracking channel is the exponential of the estimated carrier phase. Thus, a (receiver) single-difference correlator is obtained by multiplying the rover prompt correlator with the exponential of the corresponding reference station carrier phase and the broadcast navigation data bit.

This principle extends to double (receiver and satellite) differences and is described in greater detail later in this article. The signal dynamics in a double-difference correlator can be very low. For example, for a static user and baseline length of 50 meters, the remaining acceleration is around 50 micrometers/second². Thus, we can form coherent batches of several hundreds of seconds and use those batches to estimate the double-difference carrier phase. (In our test we used batches of a maximum of 90 seconds.)

Ideally, the double-difference correlators within one batch represent a tone signal, and the frequency is the (double-difference) Doppler frequency. The phase of the tone signal relates to the user position. An adaptive filter detects the dominant frequency contribution of the line-of-sight signal and applies a linear filter. Ideally, only the line-of-sight signal passes through and multipath signals (having a slightly different Doppler) and noise are filtered out.

The frequency selectivity is inversely

proportional to the batch length. In our approach the separation of those components takes place entirely in the frequency domain, whereas a conventional PLL smoothes carrier phase estimates in the time domain. Finally, an estimator derives the Doppler frequency and the carrier phase at a given reference epoch from the filtered signal and writes them into a RINEX file. This process includes unwrapping and undoing the differencing process with certain assumptions on the receiver clock.

A typical standard PLL works with a tracking loop bandwidth of 5–15 hertz to cope with user oscillator variations, even if the receiver is operated in a static mode. In contrast, a batch length of 90 seconds corresponds to an equivalent loop bandwidth of 5.6 millihertz. Provided that the tracking channel can maintain code and Doppler lock (e.g., via aiding from other channels for vector tracking), then we will show that a carrier tracking sensitivity of well below zero decibel-hertz is possible.

In forests, the canopy attenuates the GNSS signals and causes diffuse scattering. Tree trunks cause the signals to creep around them, causing an extra delay. Whereas standard receivers generally cannot track the signal without cycle slips inside forests, difference correlator tracking is stable and potentially allows use of the carrier phase for precise positioning even for satellites tracked at low elevation angles.

Difference correlators also partly allow for indoor carrier phase positioning. Phase delays caused by the penetration of building materials determine the accuracy limit. This article proposes a method to identify time windows with approximately constant delays. L1 C/A and L2CM indoor data show periods of, for example, 16 minutes, where propagation delays remain within a few centimeters variation.

Using this method, we can compute an indoor position using carrier phases only (no code pseudoranges) with an accuracy of one meter.

The difference correlator concept may also find applications for attitude systems with multiple antennas or for

possible use on board spacecraft, which receive GNSS signals at very low power levels.

Difference Correlator Concept

Single- and double-difference observations (code and carrier) are well-known concepts in precise positioning that are used to eliminate common-mode errors. Difference correlators extend these concepts to the level of correlator values. By doing this, the same common-mode errors cancel out, thereby drastically reducing the signal dynamics.

Applying longer filter times reduces the noise and eliminates multipath contributions. A simpler version of difference correlators was introduced in Chapter 10 of T. Pany's book, *Navigation Signal Processing for GNSS Software Receivers* (see the Additional Resources section at the end of this article), and will be summarized here.

Forming Differences. At the correlator level forming differences is a little tricky, because various (equivalent) ways to define the carrier phase inside the receiver are available and because the timing relationship of the data is important. The following discussion describes the methods of single-difference forming and double-difference forming as well as how undifferenced observations are then re-derived from these formed differences.

Single-Difference Observations.

Generally the classical receiver single-difference carrier phase observation is defined through an equation such as the following:

$$\Delta\varphi^k(t^k) = \varphi^{k,rov}(t^k) - \varphi^{k,refk}(t) \quad (1)$$

where,

$\varphi^{k,rov}$ is the rover carrier phase to satellite k [radians]

$\varphi^{k,refk}$ is the reference station carrier phase to satellite k [radians], and

$\Delta\varphi^k$ is the single-difference carrier phase to satellite k [radians].

The carrier phases are read from a RINEX file or a similar source (e.g., RTCM). The epoch t^k generally refers to the receiver timescale. Note, the timescales do not match exactly, but those timing errors between receiver

clocks can be tolerated if satellite position calculation properly accounts for these differences.

Single-difference Correlator. Forming correlator differences requires a slightly different approach. First, the tracking channel outputs a carrier phase reading based on the internal numerically controlled oscillator (NCO), which is not necessarily under the control of a PLL. Typically, we use a frequency-locked loop (FLL) or vector tracking methodology for this purpose.

In general, the internal tracking is not locked to the received carrier phase (due to poor signal conditions), and the prompt correlator contains the difference between the received and internal carrier phase. Estimating the received rover phase follows expression such as:

$$\exp\{i\varphi^{k,rov}(t)\} = |a(t)| \exp\{i\varphi^{k,NCO}(t)\} P^{k,rov}(t) \quad (2)$$

where,

$a(t)$ is the inverse signal amplitude (not relevant here), $\varphi^{k,NCO}$ is the rover carrier phase to satellite k [radians] based on NCO reading while using internal (e.g., FLL) tracking, and $P^{k,rov}$ is the rover prompt correlator (complex valued) capturing the difference between the internal tracking and the true received signal.

Therefore, a receiver single-difference correlator is written as

$$\Delta P^k(t^k) = \exp\{i\varphi^{k,NCO}(t^k)\} P^{k,rov}(t^k) \exp\{-i\varphi^{k,ref}(t^k)\} d(t_{sent}^k) \quad (3)$$

where,

d is the broadcast navigation data bit (if any) and ΔP is the single-difference correlator.

To wipe off data bits we retrieve the broadcast data bit from the reference station corresponding to the sent time for the correlator value $P^{k,rov}$. We assume that the internal receiver time t^k is steered towards the true GPS time within plus or minus one millisecond and that the same applies for the reference receiver. Then we simply take t^k (which is a rover time) and use it as a reference station time to extract the reference station carrier phase.

Using Equation (5), this process is later reversed, thereby compensating for any timing error in the range.

Applying a filter F (see next section) to batches of single-difference correlator values allows the phase of the filtered correlator values to be unwrapped, thus:

$$\Delta Q^k(t) = F\{\Delta P^k(t)\} = |\Delta Q^k(t)| \exp\{i\Delta\eta^k(t)\} \quad (4)$$

where,

ΔQ^k is the filtered single-difference correlator

F is the batch filter, and

$\Delta\eta^k$ is the unwrapped phase of the filtered single-difference correlator [radians].

Finally, adding the unwrapped phase to the reference station phase yields the new improved undifferenced rover carrier phase, which is then written into the RINEX file or used otherwise:

$$\varphi^{k,rov}(t) = \Delta\eta^k(t) + \varphi^{k,ref}(t) \quad (5)$$

The computation of (3) requires the evaluation of the reference station carrier phase at the rate of the correlator values (e.g., 50 hertz). The phase itself is typically available with a lower rate (e.g., 1 hertz). Therefore, a suitable interpolation procedure must be used.

Double-Difference Correlator. The double-difference process forms satellite differences between two single-difference correlators. The reference satellite has the index l . It is typically the satellite with the highest elevation.

The double-difference correlator is written as

$$\nabla\Delta P^{k,l}(t^k, t^l) = \Delta P^k(t^k) \overline{\Delta P^l(t^l)} \quad (6)$$

where,

t^k is the other satellite epoch in [seconds] when a correlator value for the satellite k is available,

$\nabla\Delta P$ is the double-difference correlator,

l is the reference satellite index, and

k is the other satellite index.

Equation (6) depends on the two epochs of the two single-difference correlators involved. Typically we choose these as the timely nearest correlator values. The later undifferencing process — indicated in Equation (9) or (10) — will eliminate any errors introduced by asynchrony of the correlators for satellites k and l .

Applying the adaptive filter F to the double-difference correlator values unwraps the resulting phase:

$$\nabla\Delta Q^{k,l}(t) = F\{\nabla\Delta P^{k,l}(t)\} = |\nabla\Delta Q^{k,l}(t)| \exp\{i\nabla\Delta\eta^{k,l}(t)\} \quad (7)$$

where,

$\nabla\Delta Q$ is the filtered double-difference correlator,

F is the batch filter, and

$\nabla\Delta\eta^{k,l}$ is the unwrapped phase of the filtered double-difference correlator [radians].

Undoing Double Differencing. GNSS data format standards like RINEX are only defined for undifferenced observations. Retrieving single-difference (and finally undifferenced) observations from the double-difference phase is not straightforward because the receiver clock error has been completely eliminated during the double-difference process. The following paragraphs propose two methods with which to reintroduce the receiver clock error. For any positioning processing, this error has to be taken into account again and then, respectively, removed. The only important thing is that a relationship remains intact between the carrier and range clock within the receiver.

If a strong satellite signal is available, its carrier phase might be estimated with the single-difference approach or via undifferenced data. We then obtain the single-difference carrier phase of the other satellites by adding the double difference to the reference single difference. Finally, the undifferenced observations are obtained when the carrier phases of the reference station are added:

$$\varphi^{k,rov}(t^k) = \nabla\Delta\eta^{k,l}(t^k, t^l) + \Delta\eta^l(t^l) + \varphi^{k,ref}(t) \quad (8)$$

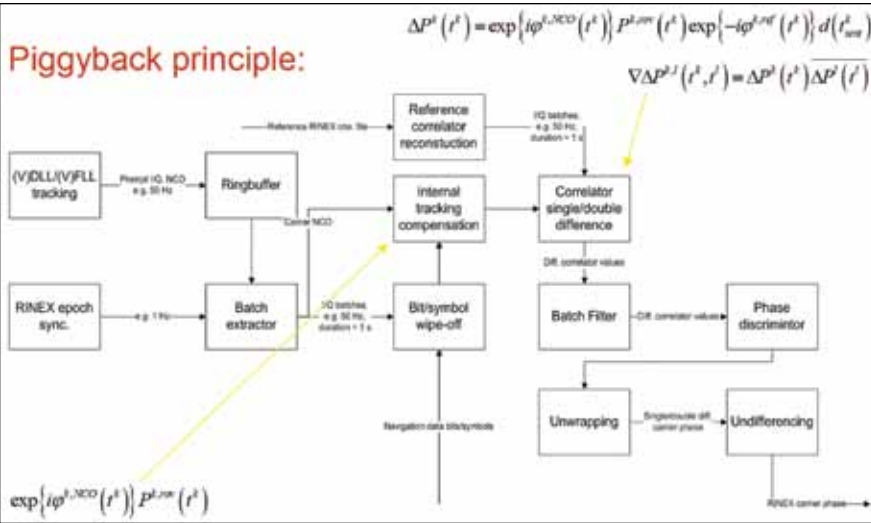


FIGURE 1 Block diagram of the difference correlator tracking scheme

If single or undifferenced tracking cannot be applied for the reference satellite, then we may choose to derive the carrier phase of the reference satellite from the code pseudorange. The undifferenced carrier phase of all satellites is given by

$$\varphi^{k, rovr}(t^k) = \nabla \Delta \eta^{k,l}(t^k, t^l) + \frac{2\pi}{\lambda} R^{l, rovr}(t^l) - \varphi^{l, ref}(t^l) + \varphi^{k, ref}(t^k) \quad (9)$$

where,

$R^{l, rovr}$ is the code pseudorange of rover for reference satellite and λ is the carrier wavelength [in meters].

Again, this calculation needs to be performed to get the standard RINEX output. In future research, the RTK positioning will have to be adapted and allow the direct use of these double-difference correlator observations. In RTK positioning any error introduced into the undifferenced carrier phase values due to the use of the code pseudorange via Equation (9) will cancel. If the positioning algorithm works with undifferenced carrier phases, then errors introduced by (9) will affect the carrier phase-based receiver clock estimate. The artificially introduced receiver clock error directly relates to the code pseudorange accuracy of $R^{l, rovr}$.

Block Diagram

We implemented the difference correlator scheme using the application programming interface (API) of the software receiver in a postprocessing mode (as was described, for example, in the article by T. Pany *et alia* listed in Additional Resources). The first step captures rover signal samples for L1 and L2 as well as reference station observations in RINEX format for L1 C/A and, eventually, L2C plus the broadcast navigation data bits. In a second step all these data are processed, resulting in a RINEX file with the rover observations.

Currently, the difference correlator scheme applies only for carrier tracking. Rover code and Doppler observations are produced using standard tracking loops with vector DLL (VDLL) or vector FLL (VFLL). The implemented difference correlator scheme is generally real-time capable, but at this time reference

station data is read in via a RINEX file. For real-time operation, RTCM could be used.

Figure 1 shows a block diagram of the difference correlator together with the key formulas of the preceding section.

The difference correlator mode works as a piggy-backed module on top of the standard rover tracking. We realize this through either DLL/FLL channels or a vector tracking loop (VDLL/VFLL). The tracking channels output prompt I/Q correlator values for all tracked signals, which are stored in buffers. Batches (synchronized to the RINEX observation rate) are formed out of the buffers. For each batch, the effect of the internal tracking is compensated, as indicated by Equation (2).

The reference station carrier phase is interpolated to the rover epoch, the data bit is retrieved from the assistance data base, and the difference correlator is formed, as shown in (3) or (6), respectively. We then feed the batches of difference correlator values into a batch filter. Using these filtered difference correlator values, the phase discriminator estimates the wrapped phase and the Doppler.

The wrapped phase is compared to the wrapped phase estimate from the previous batch at the boundary epoch, thereby obtaining the unwrapped carrier phase. The difference of the two phase estimates should be near an integer value and, if not, is an indication that a cycle-slip occurred. Finally, we apply undifferencing, and the carrier phase is written together with the conventional code and Doppler observations into the RINEX file.

Batch Processing

Within a batch, whose length equals the RINEX observation rate, the difference correlator values are analyzed coherently. In this step, we can use dedicated filters to reduce the noise and multipath. The filters rely on the fact that usually only the line-of-sight signal behaves in a deterministic way and shows up as a clear peak in the spectrum. Noise and multipath have a more random character and appear throughout the entire spectrum.

Correlator Batch Filters. The batch filter was introduced earlier in equations (4) and (7). Here, we now offer a detailed description.

Generally, the filter F has the form

$$Q(t_\mu) = F\{P(t_\mu)\} \quad (10)$$

and converts raw correlator values P into filtered correlator values Q . The filter may work with undifferenced values, or single or double differences. We will discuss two options here: the cost minimization filter and the frequency domain filter.

Cost Minimization Filter. The cost minimization filter first fits a quadratic phase model to the batch of correlator values.

$$\hat{\varphi}, \hat{f}, \hat{a} = \arg \min_{\varphi, f, a} \sum_{\mu} \left(1 - \cos \left(\arg \left\{ P(t_\mu) \exp \left\{ -i \left(2\pi f t_\mu + 2\pi a t_\mu^2 + \varphi \right) \right\} \right\} \right) \right) \quad (11)$$

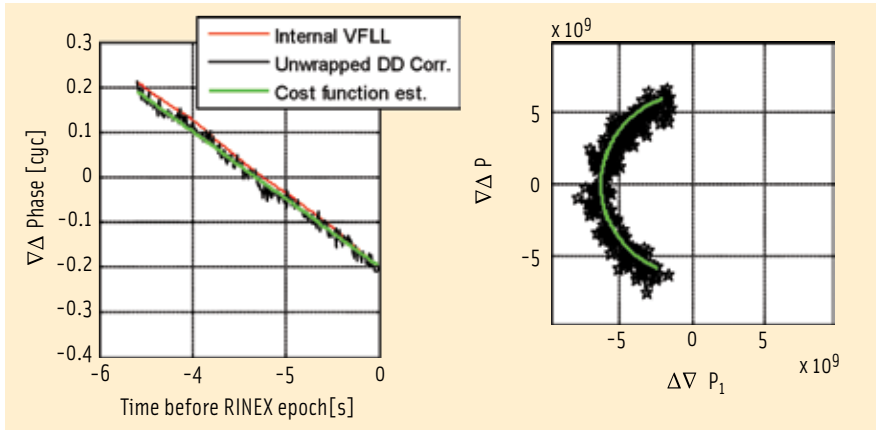


FIGURE 2 Two clearly visible GPS C/A satellites over 5 seconds and 20 milliseconds primary coherent integration time; left: estimated double-difference carrier phase with various methods; right: double-difference correlator values plus cost minimization fit

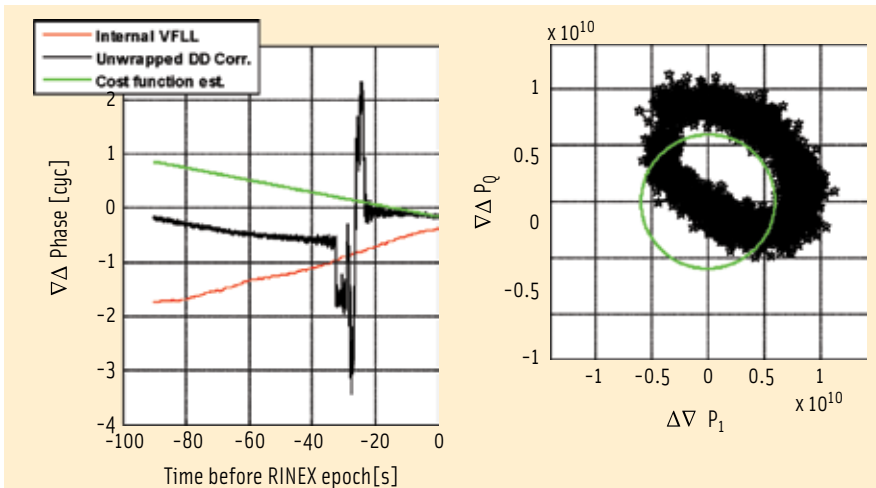


FIGURE 3 One fully visible GPS C/A satellite (PRN 3 of the canopy test) and one canopy-attenuated satellite over 90 seconds and 20 milliseconds primary coherent integration time; left: estimated double-difference carrier phase with various methods; right: double-difference correlator values plus cost minimization fit

where

φ is the carrier phase offset [radians], f is the Doppler frequency [hertz], and a is the acceleration [hertz/second].

A caret or “hat” above a symbol denotes an estimated parameter. The admissible range for Doppler and acceleration values can be limited based on prior knowledge of the line-of-sight dynamics and generally depends on the baseline length.

The estimation itself is carried out with a grid search algorithm for Doppler and acceleration. For fixed Doppler and acceleration values, the phase can be calculated analytically.

Based on the estimated parameters, the filtered correlator values are given by

$$Q(t_{\mu}) = \exp \left\{ i \left(2\pi \hat{f} t_{\mu} + 2\pi \hat{a} t_{\mu}^2 + \hat{\varphi} \right) \right\} \quad (12)$$

Figure 2 shows an illustration of the cost minimization filter with real data. On the right-hand side, the raw double-difference correlator values P appear as black stars and the green line is the best fit to these. A time span of five seconds is considered.

Due to the satellite motion, the double-difference carrier phase changes by approximately one-third of a cycle (the numerical value of the phase change is geometry/baseline length dependent). The signal power is high and nearly constant. The raw values apparently lie on a circle centered at the origin. Simple unwrapping of P would also give the

correct phase estimate as shown on the left hand side.

If the transmissions from one of the satellites are attenuated, a different situation may occur, as in Figure 3. In this example the raw correlator values form approximately a circle centered at $(0.23 + i \cdot 0.21) \times 10^{10}$. This mean value corresponds to one propagation path near 0 hertz, the circle to the presence of another propagation path at 1/90 seconds (~ 0.01 hertz). Both paths have similar amplitudes, and the total signal power nearly cancels at some epoch. Fading occurs and simple unwrapping introduces cycle slips. However, the cost minimization filter correctly identifies a continuous carrier phase (corresponding to the second propagation path with 0.01 hertz).

Frequency Domain Filter. The estimation in the frequency domain first multiplies the correlator values by a proper windowing function, h (e.g., a Hamming window).

$$P'(t_{\mu}) = P(t_{\mu})h(t_{\mu}) \quad (13)$$

Eventually, the processing increases the vector length via zero-padding to achieve a better frequency solution, and the Fourier transform is computed.

$$\tilde{P}(f) = FFT \{ P' \} \quad (14)$$

Figure 4 shows a time series of spectra based on Equation (14). The position of the peak corresponds to the double-difference Doppler and the complex argument of the peak to the double-difference carrier phase. If long integration times are used, the peak is clearly visible even if one or both signals is/are highly attenuated. Figure 4 uses an integration time of 90 seconds. This ultra-long integration time allows the separation of line-of-sight and multipath signals for low-elevation-angle satellites.

In the figure, the turquoise line clearly shows two peaks corresponding to two propagation paths. The brown and beige lines correspond more to a single propagation path. In the case of the other two lines (green, black), the frequency separation is not high enough to show up as separate peaks; instead, the main peak broadens.

$$\text{var} \langle \varphi \rangle < \left(\frac{\pi}{6} \right)^2 \tag{16}$$

Figure 5 plots carrier phase noise as a function of the carrier-to-noise ratio (C/N_0) for different values of T_{coh} . For a static user and an integration time of 30 seconds, extremely low C/N_0 values seem to be possible. In that case, we gather enough energy before computing the discriminator, and the long integration time ensures high Doppler estimation accuracy.

Of course, code, and Doppler lock must be maintained, for example, via vector tracking. In vector tracking, at least four signals with higher power force another channel to lock onto a very low power signal of, for example, -3 decibel-hertz. The case of 20 milliseconds corresponds to standard phase tracking of a pilot signal.

Field Trials: Signal Processing Results

This section summarizes the results from tests conducted during two trials in forest and indoor environments.

Canopy Test. For the canopy test, a geodetic-quality rover antenna was placed on a tripod inside a forest as shown in Figure 6. The experiment took place on December 1, 2011, tracking satellites over the course of half an hour.

A large part of the deciduous forest where the test took place had already dropped most of its leaves. Nevertheless, the forest is quite dense and frequent “shadowing” (signal obstructions) due to trunks and branches was expected. With an antenna splitter, the signal was fed into the RF front end of the multi-GNSS software receiver to record the GPS L1 signal samples and into a commercial geodetic receiver used for comparison. The reference station was located 2.477 kilometers away from the observatory Graz/Lustbühel, Austria.

Signal Processing Results. Code and Doppler vector tracking based on 20 millisecond-long coherent integrations was used to track all visible satellites at the rover. The estimated signal power at the rover varied from 5 to 51 decibel-hertz as shown in Figure 7. Values below 10-15 decibel-hertz occur for the low-elevation-angle satellites.

Reference station RINEX data and navigation data bits were fed into the double-difference correlator module to process the rover data with settings as shown in Table 1. We chose PRN11 (GPS space vehicle number 46) as the reference satellite.

Figure 8 shows a typical example of the estimated double-difference correlator phase. Each batch interval produces an

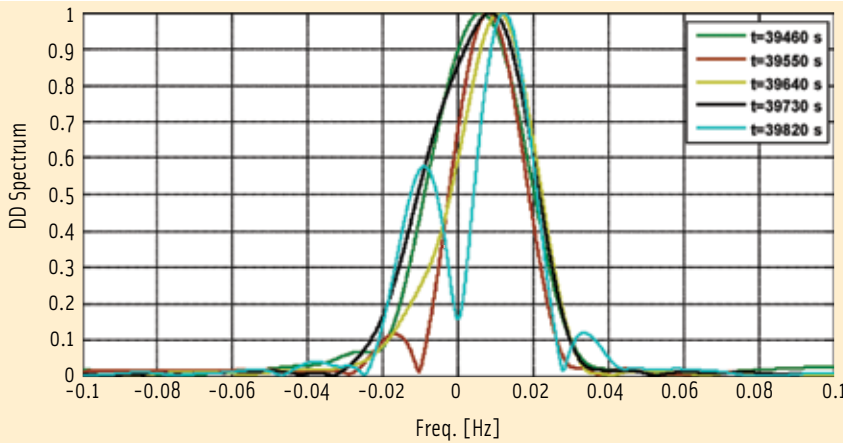


FIGURE 4 Consecutive double-difference spectra for a low elevation satellite (PRN 3 of the canopy test); the black line corresponds to Figure 3

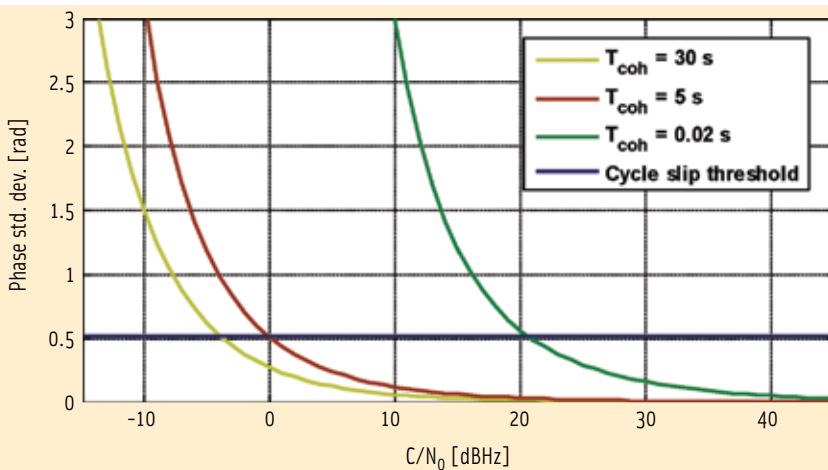


FIGURE 5 Carrier phase noise for a double-difference correlator with different coherent integration times plus rule-of-thumb cycle-slip threshold

Sensitivity. Assuming that the reference satellite and the reference station data have virtually no noise, we can approximate the variance of a double-difference correlator as follows:

$$\text{var} \langle \varphi \rangle = \frac{1}{2T_{coh} C/N_0} \left(1 + \frac{1}{2T_{coh} C/N_0} \right) + \frac{T_{coh}^2}{4} \left[\left(\frac{6}{T_{coh}^3} \right) \left(1 + \frac{1}{T_{coh} C/N_0} \right) \right] \tag{15}$$

where,

$\text{var} \langle \varphi \rangle$ is the double-difference carrier phase variance difference correlator [radians²],

T_{coh} is the coherent integration time [seconds], and C/N_0 is the power of the weak satellite [hertz].

The phase noise is the sum of the phase discriminator noise, the first term (here the Cramér-Rao lower bound is used), and a second term related to the interpolation of the phase values to the measurement epoch. The latter term is the product of the interpolation time ($T_{coh}/2$) from the midpoint of the batch interval to the boundary, multiplied with the angular frequency ($2\pi * \text{Doppler}$) Cramér-Rao lower bound.

For cycle-slip free unwrapping, a six-sigma criterion is applied, as in E. D. Kaplan’s and C. Hegarty’s famous book,



FIGURE 6 Measurement location and sky plot for the canopy test

Parameter	Value
Code/Doppler tracking scheme	VDLL/VFLL
Carrier tracking scheme	Double
Integration time	5 s
Overlap	0.2 s
Carrier phase estimation	Cost function
Max/Min Doppler	+/- 5 Hz
Doppler grid points	801
Max/Min acceleration	+/- 0 Hz/s
Acceleration grid points	-

TABLE 1. Canopy test processing parameters

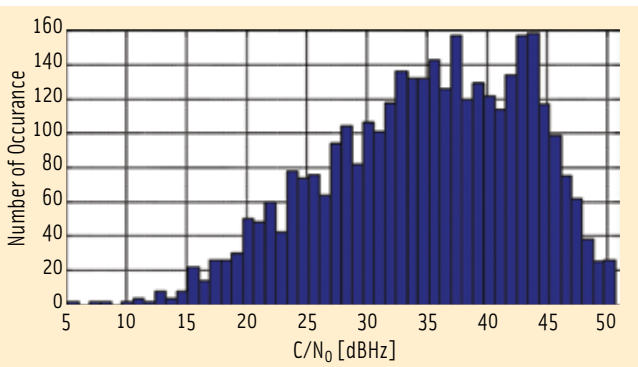


FIGURE 7 Histogram of the measured C/N_0 values at the rover during trial under forest canopy

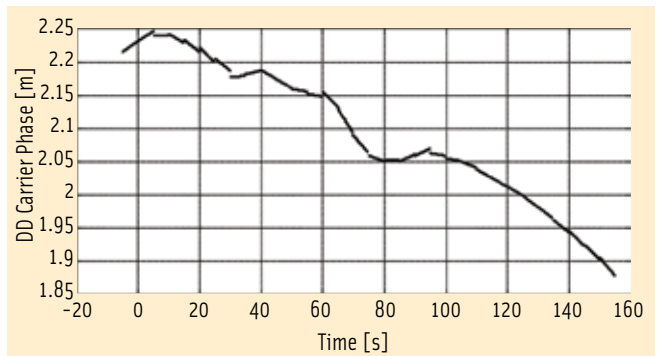


FIGURE 8 Double-difference carrier phase of PRN 28 (reference PRN 11), $t_0 = 13:50:40$, after subtracting a linear trend of 2.299 hertz

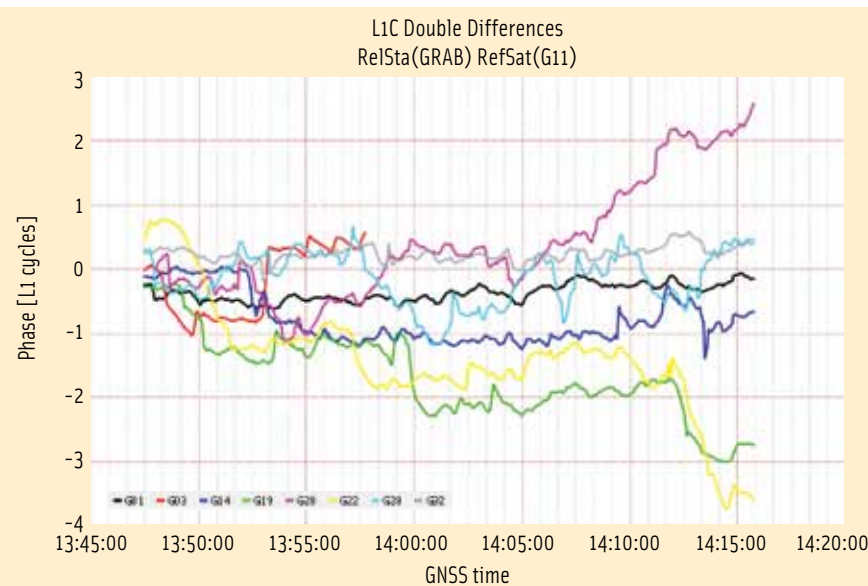


FIGURE 9 Double-difference carrier phase (reference station – rover, reference satellite PRN 11) with the multi-GNSS software receiver based on double-difference correlator tracking (Integer ambiguity resolution is applied for better plotting. Note: In the figure legend, the terms G01, G03, and so forth are the PRN numbers according to the RINEX convention.)

fit to each other in the sense that the mismatch at the batch boundaries is only a few millimeters. We conclude that the estimates are truly a measurement of the incoming electromagnetic wave and are not, for example, the artifact of signal processing. An artifact would show up as pure noise, with mismatches within +/- 0.5 cycle.

The double-difference carrier phase reflects the geometric motion of satellites, atmospheric delay variations, and propagation delay changes due to trunks, branches, and canopy (multipath, diffuse reflections or refractions). In Figure 9 two high-elevation-angle satellites (PRN1 and PRN32) are quite smooth (together with the reference satellite).

Other medium- and high-elevation-angle satellites (PRN14, PRN19, PRN20, PRN22, and PRN28) have more noise and show multiple plateaus. Plateau changes are caused because the received electromagnetic wave behaves this way and not because the phase tracking “slips”. Otherwise plateau changes are

estimate of the Doppler frequency and carrier phase. The overlap between the different batches is small (0.2 second)

and estimation outputs can be considered as uncorrelated.

Doppler and carrier phase estimates

similar to cycle slips, but the numerical value of the slips is small.

Very low-elevation-angle (<10 degrees) satellites PRN3, PRN6, and PRN17 are not shown (see Figure 6). These may have been influenced by the topography and displayed significant drifts.

The rover coordinates were obtained from a float solution using the time span 14:00–14:10. Figures 9 and 11 use the same coordinates for the rover and also for the commercial receiver.

Figure 10 compares the zero-baseline double-difference carrier phase values of the commercial receiver results with those processed with the difference correlator (commercial receiver — difference correlator). Every time the commercial receiver outputs L1 carrier phase values, the double-difference carrier phase is near an integer (+/-0.04 cycle). This confirms the correctness of the double-difference carrier phase tracking algorithm.

Due to the difference correlator's high sensitivity, it also provides carrier phase values when the commercial receiver loses carrier lock. For example, PRN 32 shows two large gaps for the commercial receiver (as shown by the yellow line of Figure 10). The double-difference carrier phase for PRN32 is continuous (the gray line in Figure 9).

One can argue that the data within the gaps is also useful. If the double-difference phase shows larger variations (e.g., the blue line for PRN 14 in Figure 9) it is not clear *a priori* if the double-difference correlator correctly bridges the gaps where the commercial receiver loses lock (blue line in Figure 10). In fact, Figure 9 suggests that most gaps of PRN14 are bridged correctly, but around 13:53 a plateau change occurs even for the difference correlator.

For comparison, we processed the recorded IF samples again with the software receiver, but this time using standard GPS C/A tracking parameters. A coherent integration time of 20 milliseconds was used, along with a second-order Costas PLL (no data bit aiding) with a noise bandwidth of 9 hertz

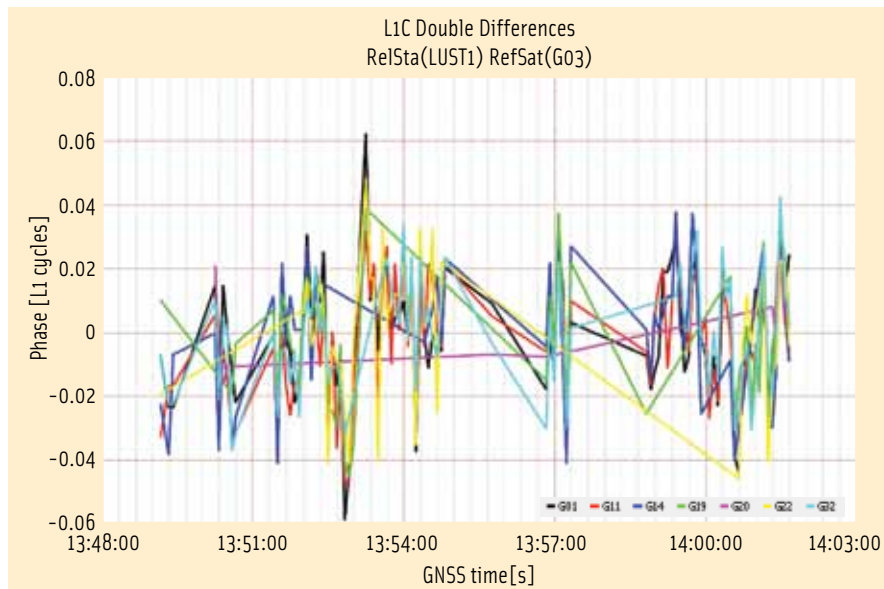


FIGURE 10 Zero-baseline (commercial – difference correlator) double-difference carrier phase (reference PRN 3), tracking (an integer ambiguity resolution is applied for better plotting.)

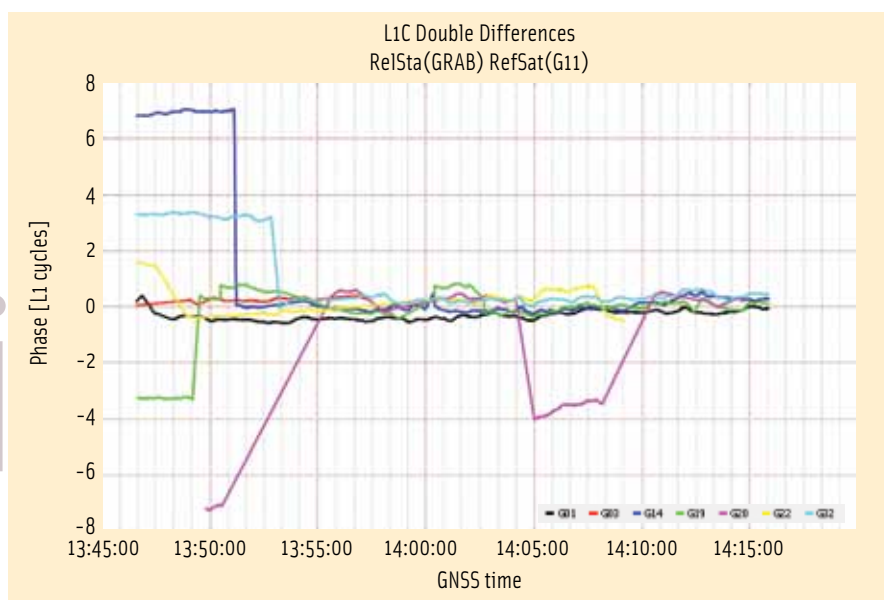


FIGURE 11 Best period of double-difference carrier phase (reference station – rover, reference PRN 11) with the commercial receiver; an integer ambiguity modulo 10 is applied for better plotting

and a second order DLL with a noise bandwidth of 0.2 hertz. Frequent cycle slips occur on all satellites apart from PRN11. Every time a cycle slip occurs, the receiver has to decode a GPS C/A navigation message preamble to resolve the 180-degree ambiguity.

Overall, the obtained carrier phase appears heavily disrupted. The data of the commercial receiver displayed qualitatively the same behavior as indicated by the results in Figure 10. In part, large

carrier phase outages occur together with frequent cycle slips. However, a few minutes with relatively stable phase tracking appear in Figure 11. Nevertheless, even this period is corrupted by several cycle slips. Those slips are typically very large (thousands of cycles), whereas the cycle slips of the difference correlator are small (one or two cycles).

This data was used for positioning. The obtained position did allow us to plot the double-difference carrier phase

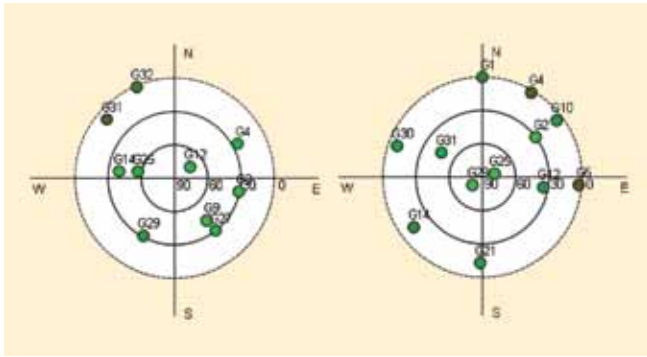


FIGURE 12 Skyplot at the beginning (left) and end (right) of the L1/L2 indoor experiment

residuals (Figures 9 and 11). A visual inspection demonstrates that the residuals have nearly no slope and the phase values are near an integer. Thus, the position is somehow reasonable.

On the other hand, the difference correlator data is contaminated with measurements that are influenced by severe propagation degradations. Those data portions must be eliminated first, before the difference correlator can be used in an RTK algorithm trying to fix the ambiguities. Further trials with dual frequency L1/L2 data might give more insight into how the additional tracking stability of the difference correlator could be optimally exploited for positioning inside forests.

Indoor Test

Based on the good performance achieved in the forest, we also wanted to test our method in a moderate indoor environment. The need for precisely surveyed indoor reference points became obvious. Only with their help, would it be possible to judge the precision of the car-

rier phase measurements. Therefore, IFEN requested that a surveying office measure the coordinates of the indoor points together with the coordinates of the two roof antennas with theodolites. All coordinates have a precision of approximately 0.5

centimeter relative to the roof antennas.

For the indoor L1/L2 experiment, we placed the antenna phase center 1.651 meters above Point 133 inside the office and used an outside antenna above the Point IFEN2 as the reference station with open-sky conditions. Approximately two hours of data were collected during a period when four L2C-capable satellites (PRNs 12, 25, 29, and 31) were visible.

The office has a window to the north of Point 133. The elevation angle of the upper window border is approximately 25 degrees. The window is not facing to reflecting surfaces. Therefore, we can safely assume that all satellites having an elevation higher than 25 degrees had to penetrate at least one wall/ceiling prior to reception by the indoor antenna.

Figure 12 shows skyplots of the satellite configurations at the beginning and end of the indoor test.

Data Processing. We postprocessed the gathered data in the usual way. Table 2 summarizes the processing parameters.

Results. A typical good result of the

carrier tracking performance is that of PRN25 with PRN12 used as the reference satellite. Both signals penetrate the ceiling to reach the indoor antenna. As can be seen from Figure 13, the L1 and L2 carrier phase estimates are highly consistent and reflect the geometric motion of the satellite. Doppler (slope) and phase estimates are also consistent, and the signal processing did not detect any cycle slips.

The only difficult period occurred around the time interval 3450–3600 seconds on L2CM. During this time, fading on L2 occurred, as can be seen in the right-hand part of Figure 13. However, the spectrum of the double-difference correlator still shows a clearly visible peak, and we argue that the estimates are not corrupted by excessive noise, as reflected in the snapshot of the double-difference correlator spectrum presented in Figure 15.

However, the L2 estimates experience some sort of a cycle slip (or plateau change) as shown in Figure 14. The plateau change develops over a period of around 100 seconds during which the Doppler and phase estimates are slightly less consistent than during normal tracking. The 30-second batches still show phase gaps of less than two centimeters at the boundaries, and the signal processing does not detect them as cycle slips.

Another good satellite combination was obtained from PRN29 (reference PRN12) with the results shown in Figure 16. Again, both satellite signals are received through the ceiling of the room

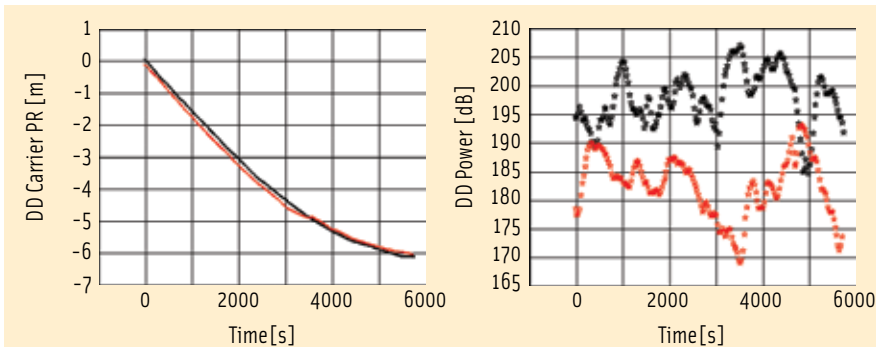


FIGURE 13 Double-difference carrier phase and signal amplitude for PRN25 (reference PRN 12) on L1 C/A (black) and L2CM (red)

Parameter	Value
Code/Doppler tracking scheme	VDLL/VFLL
Carrier tracking scheme	Double
Integration time	30 s
Overlap	0.2 s
Carrier phase estimation	Cost function
Max/Min Doppler	+/- 0.05 Hz
Doppler grid points	81
Max/Min acceleration	+/- 0.0001 Hz/s
Acceleration grid points	41

TABLE 2. Indoor processing parameters

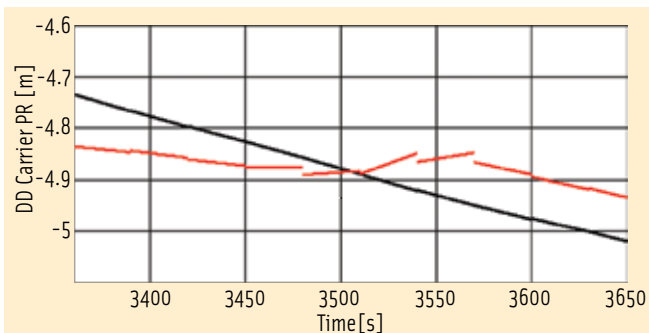


FIGURE 14 Zoom into Figure 13, showing some kind of cycle slip (plateau change) on L2 (red)

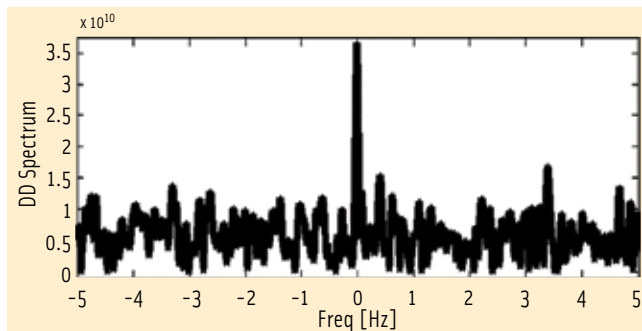


FIGURE 15 L2CM double-difference correlator spectrum (black) at $t = 3540\text{--}3570$ of Figure 8

in which the receiver antenna was located.

Using the known (pre-surveyed) coordinates, we were able to subtract the geometric distance from the double-difference carrier phase observations and plot the results for the wide-line linear combination. This puts us in a position to identify useable data portions (these are section without plateau changes or real cycle slips).

If this technique is used for real indoor positioning, however, we do not know the coordinates of the rover accurately (as we do in a test bed situation) and thus we cannot subtract the geometric distance. Therefore, we need a different measure for identification of suitable observation sections.

Double differences of phase ranges (carrier phase observations converted to meters) of both frequencies should show similar patterns. Because the distance to the reference station in the indoor experiment were very short — only tens of meters — the ionospheric effects are completely removed.

The difference of the L2 phase range double differences minus the L1 phase range double differences are shown in Figure 17. For plotting, these metric values have been converted back to L2 cycles.

The curves of PRN12 and PRN29 are rather flat, indicating a fairly good agreement of L1 and L2 phase observations. The values for PRN31 show larger excursions. However, the signal processing for PRN31 indicated severe tracking problems, which appear in the plots.

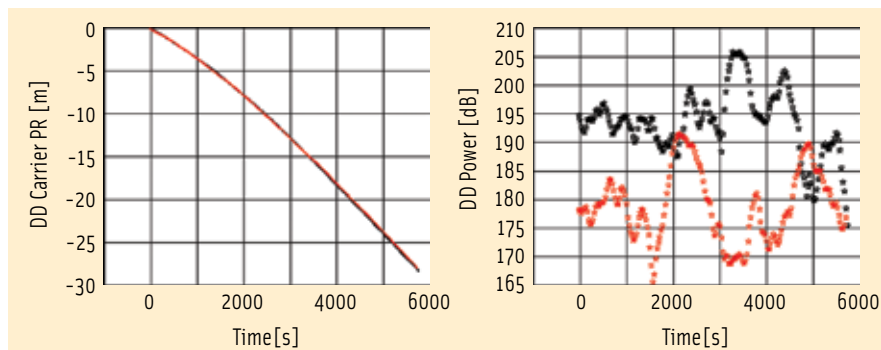


FIGURE 16 Double-difference carrier phase and signal amplitude for PRN29 (reference PRN 12) on L1 C/A (black) and L2CM (red)

Overall, one can identify two rather good sections, one of 10 minutes at 346300–346900 seconds and another of about 16 minutes at the end of the test (347310 to 348270 seconds).

Interpretation. This static L1/L2 indoor test verifies the ability of the difference-correlator method to track the carrier phase of indoor signals. The method, however, also potentially may track reflected signals very stably. A consistency analysis of L1 and L2 data might be used as a decision criterion to check the validity of the data.

With the known geometry, we can investigate biases on the double-difference carrier phases. Strong biases seem to be present and they could be well explained by refractivity variations

of the penetrated building materials. For example, the article by G. Hein *et alia* (Additional Resources) predicts a propagation speed of 61 percent of the speed of light for lumber, of 49 percent for bricks, and 43 percent for concrete. Thus, delays on the order of the wavelength are easily possible. Furthermore, reflections at the wall boundaries complicate the problem.

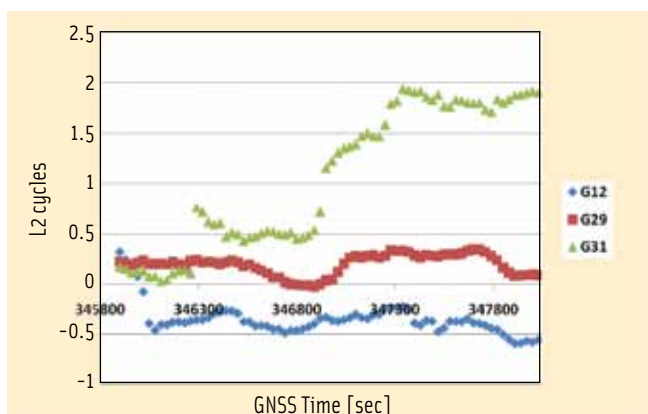


FIGURE 17 L2 double-difference phase ranges minus L1 double-difference phase ranges converted to L2 cycles

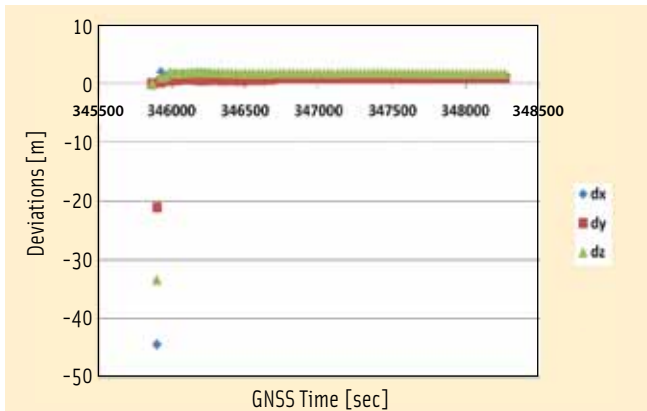


FIGURE 18 Coordinate convergence for floating ambiguity computation; time interval 345870 to 348270 seconds

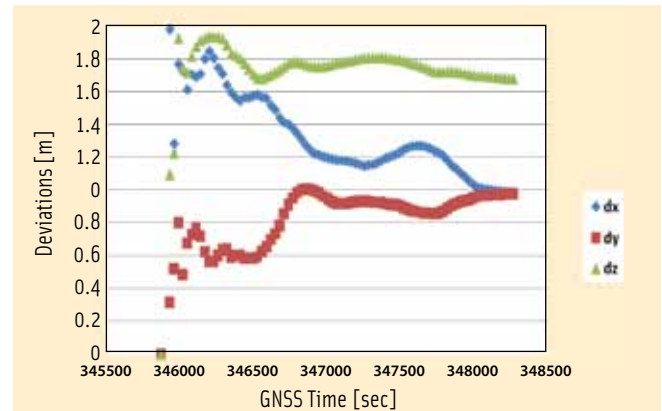


FIGURE 19 Coordinate convergence for floating ambiguity computation; time interval 345870 to 348270 (first epochs removed)

Use in Indoor Positioning

The carrier phases obtained in the indoor scenario do not have blunt jumps that would suggest the occurrence of cycle slips. Therefore, these carrier phases may provide a reasonable positioning quality.

Knowing that the pseudorange quality is not sufficient, we decided to base the positioning mainly on the carrier phases. The pseudoranges must be down-weighted drastically so that the baseline computation is effectively identical to a phase-only differential positioning. Phase-only computations are well known to rely heavily on satellite geometry changes for position determination and require therefore longer measuring intervals.

Under open sky scenarios this has been the traditional method of precise differential positioning for several decades now. The open question for us was, do the indoor observations still have enough contribution from the line-of-sight signal (to the satellite geometry itself) or is the whole dataset so contaminated by multipath reflections as to prevent any reasonable positioning result?

The carrier phase observations were processed using a proprietary software. We used all carrier phase observations available. The carrier phases on L2 were only available for PRN12, PRN25, PRN29, and PRN31. These satellites enabled us to track the L2C code. However, more satellites supported L1 carrier phase tracking. The complete carrier phase information set from satellites above an elevation mask of 15 degrees has been used in our baseline computations.

Figure 18 shows the true convergence errors of the floating ambiguity computation of the whole time interval that we analyzed. Because the computation is mainly dependent on the carrier phases, the initial positions are quite far off, but the convergence settles the results very quickly.

Figure 19 shows the same results zoomed in to highlight the epoch-to-epoch stability of the positioning. The overall deviation of the results does not improve significantly over the complete observation interval. Apart from the dx component, the deviations settle within the first 10 minutes.

As already recognized earlier, the carrier phase tracking of

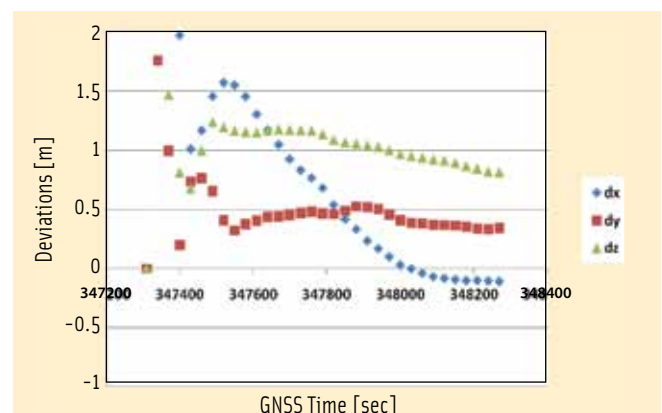


FIGURE 20 Coordinate convergence for floating ambiguity computation; time interval 347310 to 348270 (first epochs removed)

some satellites experienced difficulties during the indoor test. As discussed in our analysis of the results presented in Figure 17, the carrier for PRN31 showed some unfavorable drift in the middle of the interval. We computed the baseline with carrier phase observations limited to the two favorable sections indicated through visual inspection of the differences of the double-differenced L1 and L2 phase ranges.

The positioning results based on the last 16 minutes of the whole observation interval are given in Figure 20. The results of the first epochs have been clipped because they are outside of the plot range. These values have approximately 10–15 meter deviations, which were to be expected from our earlier computations.

Table 3 summarizes the deviations in the horizontal and vertical components to the surveyed coordinates at the end of each computation interval. The computation of the last obser-

Start	Stop	dN [m]	dE [m]	dUp [m]	Len [m]
345870	348270	-0.252	-0.752	-2.032	2.182
347310	348270	-0.566	-0.357	-0.584	0.888
346290	346890	-0.231	-1.034	-2.077	2.331

TABLE 3. Summary of indoor positioning runs

vation section of 16 minutes especially indicates that the overall length of the whole computation interval is the major contributing factor for convergence.

For the data analyzed, the convergence settled very quickly. Because the carrier phase inhibited some biases due to the penetration of the different types of materials, integer ambiguity resolution was not invoked. Our overall analysis of results suggests the need for further investigation, especially of applying difference correlator techniques to indoor positioning.

Conclusions

Difference correlators represent an effective means to remove signal dynamics from correlator values and to substantially increase the coherent integration time, thus also increasing the carrier phase cycle slip stability. The concept can be implemented as a piggyback module to conventional DLL/FLL tracking or as a preferable alternative to vector tracking (VDLL/VFLL).

Depending on the intended use, satellite or receiver single-difference correlators can be used or double-difference correlators. For static differential positioning, the use of double-difference correlators seems to be the method of choice, allowing coherent integration times of several dozens of seconds.

Our indoor test (with a batch length of 30 seconds) verifies this high tracking sensitivity. With the rover antenna on one of the reference points located in an IFEN conference room, we can continuously track the carrier phase of all satellites on L1 C/A and L2CM.

The phase and Doppler estimates based on the individual batches are highly consistent in the sense that the phase difference between the two batches relates well to the estimated Doppler. Estimates from timely adjacent batches are uncorrelated.

Indoor signals are well-known for strong multipath and fading effects. The presence of biases especially introduces challenges for position determination based on observation data tracked indoors.

Despite the fact that some of the carrier phase observations were collected indoors, these are not pure sampled arbitrary reflections of the original signals. The indoor carrier phase observations are continuous and allow the application of sophisticated differential carrier processing. The position deviations to the truth of around two meters (vertical) and, respectively, less than one meter (horizontal) are exceptionally good for the environment chosen.

The forest trials lead us to a similar conclusion. The observations are continuous and might be used with sophisticated differential carrier processing, but the handling of propagation delays is critical. Our analysis has only just started and will continue to address this as well as other issues.

Other applications in which the signal is only attenuated and biases are not introduced (e.g., strong interference, or a large distance to the GNSS satellites as might occur for a GNSS space receiver) also seem to be well suited for employing the difference correlator — and promise an easier data evaluation.

Manufacturers

The new carrier-tracking algorithm tested in the research described in this article is from **IFEN GmbH**, Poing, Germany. The processing software used in forest and indoor trials was from **inPosition gmbh**, Heerbrugg, Switzerland. The GNSS software receivers used in the tests were the SX-NSR from IFEN GmbH. The indoor test used a Zephyr 2 antenna from **Trimble**, Sunnyvale, California, USA, the forest tests an Ashtech geodetic L1/L2 701975 antenna.

Acknowledgement

The research described in this article received funding from the European Community's Seventh Framework Program (FP7/2007-2013) under grant agreement number 247866.

Additional Resources

[1] Hein, G., and A. Teuber, H.-J. Thierfelder, and A. Wolfe, "GNSS Indoors: Fighting the Fading, Part 2," *Inside GNSS*, May/June 2008

[2] Kaplan, E. D., and C. Hegarty, (eds.) *Understanding GPS: Principles and Applications*, Artech House, 2006.

[3] Pany, T., *Navigation Signal Processing for GNSS Software Receivers*, Artech House, ISBN: 978-1-60807-027-5-2010, 2010

[4] Pany, T., and B. Riedl, J. Winkel, T. Worz, R. Schweikert, H. Niedermeier, S. Iagrasa, G. Lopez-Risueno, and D. Jimenez-Banos, "Coherent Integration Time: The Longer, the Better," *Inside GNSS*, May/June 2008

Authors



Thomas Pany works for IFEN GmbH as a senior research engineer in the GNSS receiver department. In particular, he is concerned with algorithm development. He also works as a lecturer (Priv.-Doz.) at the University FAF Munich and for FH Joanneum, the University of Applied Science Graz/Austria.



Hans-Jürgen Euler studied at the Technical University of Darmstadt. He earned his Ph.D. degree on fast integer ambiguity resolution for dual-frequency GPS. After working for Terrasat (now Trimble) and Leica Geosystems, he founded inPosition gmbh in 2006. inPosition does algorithm and concept development in the area of precise GNSS positioning.



Jón Ó. Winkel has been head of receiver technology at IFEN GmbH since 2001. He studied physics at universities in Hamburg and Regensburg. He received a Ph.D. (Dr.-Ing.) from the University FAF Munich in 2003 on GNSS modeling and simulations.



Guenter W. Hein serves as the editor of the Working Papers column. He is head of the Galileo Operations and Evolution Department of the European Space Agency. Previously, he was a full professor and director of the Institute of Geodesy and Navigation at the University FAF Munich. In 2002 he received the prestigious Johannes Kepler Award from the U.S. Institute of Navigation (ION) for "sustained and significant contributions to satellite navigation." He is one of the CBOC inventors. 